Supporting Information

Effect of 2D MXene-to-Nanoparticle Ratio on the Electronic Structure of Ti_3C_2 MXene-$CsPbBr_3$ Nanocomposites

*Riya Nag, and Abhijit Bera**

Department of Physics, Midnapore College (Autonomous), Raja Bazar Main Rd, 721101

Midnapore, W.B., India

*Electronic Address: Email: abhijit.bera@midnaporecollege.ac.in

Contents

1. EXPERIMENTAL SECTION:

Materials:

Titanium aluminium carbide powder (>99%) from Nanoshel, lithium fluoride (300 mesh), ethanol, and hydrochloric acid from Merck; lead bromide (>99%), cesium bromide (>99%), N,N-dimethylformamide (>99%), oleic acid (>90%), oleylamine (>70%), toluene (>99.9%), and hexane (>95%) from Loba Chemie, Alfa Aesar, and Sigma-Aldrich, respectively. Deionized (DI) water was prepared using a Milli-Q Millipore ultrapure water filtration system. All chemicals used in this work were of analytical grade and were used as received without further purification.

Synthesis of $CsPbBr_3$ nanoparticle:

We synthesized $CsPbBr_3$ (CPB) nanoparticles in ambient conditions following a well-reported method.[1] First, we dissolved 0.4 mmol of $PbBr_2$ and 0.4 mmol of CsBr in 10 mL of N,N-dimethylformamide (DMF) under magnetic stirring for 2 hr until a uniform solution formed. Next, we added 0.6 mL of oleic acid and 0.2 mL of oleylamine to adjust the pH. After stirring for another hour at room temperature, the stock solution was ready for the next step. To precipitate the CPB nanoparticles, we quickly poured this solution into an appropriate amount of toluene, instantly forming a bright neon-yellow suspension. We then centrifuged the mixture, discarded the supernatant, and collected the sediment containing CPB precursors. To purify the sample, we repeatedly washed the sediment using hexane through centrifugation and redispersion. Finally, the purified CPB nanoparticles, which appeared to have a bright yellow dispersion, were dried in ambient conditions to obtain a fine yellow powder.

Exfoliation of Ti_3C_2 MXene:

To synthesize MXenes (MX), we followed a well-established method by selectively etching out aluminium (Al) from commercially available Ti_3AlC_2 MAX phase powder.[2] First, we prepared the etching solution by dissolving 500 mg of lithium fluoride (LiF) in 10 mL of 6 M hydrochloric acid (HCl). The mixture was stirred at 500 rpm for 15 minutes until fully dissolved. We placed the setup in an ice bath to prevent excessive heat generation before slowly adding 500 mg of MAX phase powder to the solution. The etching process was carried out at 35°C for 24 hours. Once the wet-etching was complete, we added deionized (DI) water to the black suspension and performed multiple rounds of centrifugation until the pH of the supernatant reached neutral condition. At this point, we discarded the supernatant and collected the sediment, which contained multilayer MXene. Finally, we dried the sample at 60°C and stored it in a vacuum-sealed container in the refrigerator for future use.

Fabrication of MXene-$CsPbBr_3$ Nanocomposite:

We fabricated MXene-modified $CsPbBr_3$ (CPB) composite nanomaterials using a simple solution-based method. First, we prepared a well-dispersed solution of MXene and CPB separately by adding a predetermined amount of MXene (MX) and CPB powder to water, ensuring a final 1 mg/mL concentration. This mixture was then sonicated in an ultrasonic bath for thorough dispersion. Next, we immediately combined the dark green MXene solution with the CPB solution and placed it on a magnetic stirrer at 60°C. The resulting greenish-yellow mixture was stirred continuously for 2 hours to promote uniform integration. Afterwards, we let the solution rest at room temperature for 15 minutes before centrifuging to collect the sediment. To finalize the composite, we thoroughly washed the sediment and dried it at 60°C for 2 hours under ambient conditions. The resulting greenish-yellow powder was stored for further characterization.

Fabrication and characterization of devices:

The current-voltage characterization of the device was performed using a simple configuration, where the active layer was placed between two indium tin oxide (ITO) electrodes. The ITO substrate, which was laterally etched, underwent a thorough cleaning process to remove contaminants. It was sequentially ultrasonicated in soap water, deionized (DI) water, acetone, and alcohol, spending 15 minutes in each solution to ensure complete cleanliness. After cleaning and drying well, a well-dispersed MX-CPB solution was spin-coated onto the etched ITO substrate to form a uniform active layer. The resulting film was then dried under ambient conditions before further characterization. Current-voltage (I-V) measurements were performed using a Keithley 2614B electrometer under illumination from an X2 Lab light source, with wavelength variation achieved using appropriate optical filter papers. Transient photocurrent measurements were performed by periodically modulating the illumination using a mechanical shutter placed in front of the light source.

Characterization:

Characterization of MXene-CPB composite nanomaterials was studied by X-ray diffraction (XRD), atomic force microscopy (AFM), field emission scanning electron microscopy (FESEM), energy dispersive X-ray (EDS) analysis, X-ray photoelectron spectroscopy (XPS), optical absorption spectroscopy (UV-Vis), photoluminescence spectroscopy (PL) and scanning tunneling microscopy and spectroscopy (STM and STS). These observations were investigated using Rigaku Miniflex 600 powder diffractometer, Park XE7 AFM, Zeiss FESEM, Omicron XPS, Shimadzu UV-2550 spectrophotometer, Horiba PL, and Park XE7 STM head, respectively.

STM: All STM images were acquired in constant current mode under ambient conditions using a Pt/Ir tip. The bias voltage was set between 0.5 and 1.0 V, while the tunneling current ranged from 0.04 to 0.3 nA. To analyze the electronic band gap and band structure, scanning tunneling spectroscopy (STS) measurements were performed. STS provides insights into the dependence of the tunneling current (I) and its first derivative (dI/dV) on the applied voltage. A voltage sweep at positive and negative sample bias reveals information about the conduction band (CB) and valence band (VB) of the sample, respectively. For STS measurements, the tip was positioned at a specific location on the sample surface with the feedback loop closed. The applied sample bias facilitated electron tunneling, allowing the tunneling current to be measured as a function of bias voltage. The differential tunneling conductance plotted as dI/dV versus voltage is proportional to the local density of states (DOS) at the measurement point. The STS results presented in this study represent an average of the 15–20 most frequently observed and acceptable spectra for each sample. All data were recorded at room temperature with a scan rate of 0.5 Hz.

EFM & KPFM: Electrostatic force microscopy (EFM) were performed using a Park XE-7 AFM system equipped with an external lock-in-amplifier (SR860, Stanford Research System). The topography images were taken in tapping mode in the repulsive regime. A conductive Multi75E AFM tips with resonance frequencies of 75.9 kHz were used for topography and EFM characterization. For the measurement a well dispersed sample solution was dropcasted on an n-doped Si substrate. During EFM measurements, the parameters of external lock-in amplifier' was set to: ac amplitude: 2 V, filter: 2^{nd} order, time constant: 2 ms and voltage sensitivity: 200 mV. Images were obtained at a scan rate 0.5 Hz in ambient condition.

KPFM is an atomic force microscopy-based technique that enables mapping of the local contact potential difference (CPD) between the conductive tip and the sample surface, providing information on surface potential and work function variations at the nanoscale. The same tip used for the EFM measurements was utilized for KPFM. For KPFM measurements, a spin coated thin films of the material were prepared on an indium tin oxide (ITO)-coated glass substrate. All measurements were carried out in ambient. The obtained CPD values were converted into relative work function differences using the known tip work function, enabling correlation of the electronic surface properties with the sample morphology. During KPFM mode, the lock-in amplifier's parameters were: ac amplitude: 2 V, filter: 2^{nd} order, time constant: 300 µs and voltage sensitivity: 50 mV. Images were obtained at a scan rate 0.3 Hz.

2. Characterization of MXene-CPB Nanocomposite

a) Optical Characterization

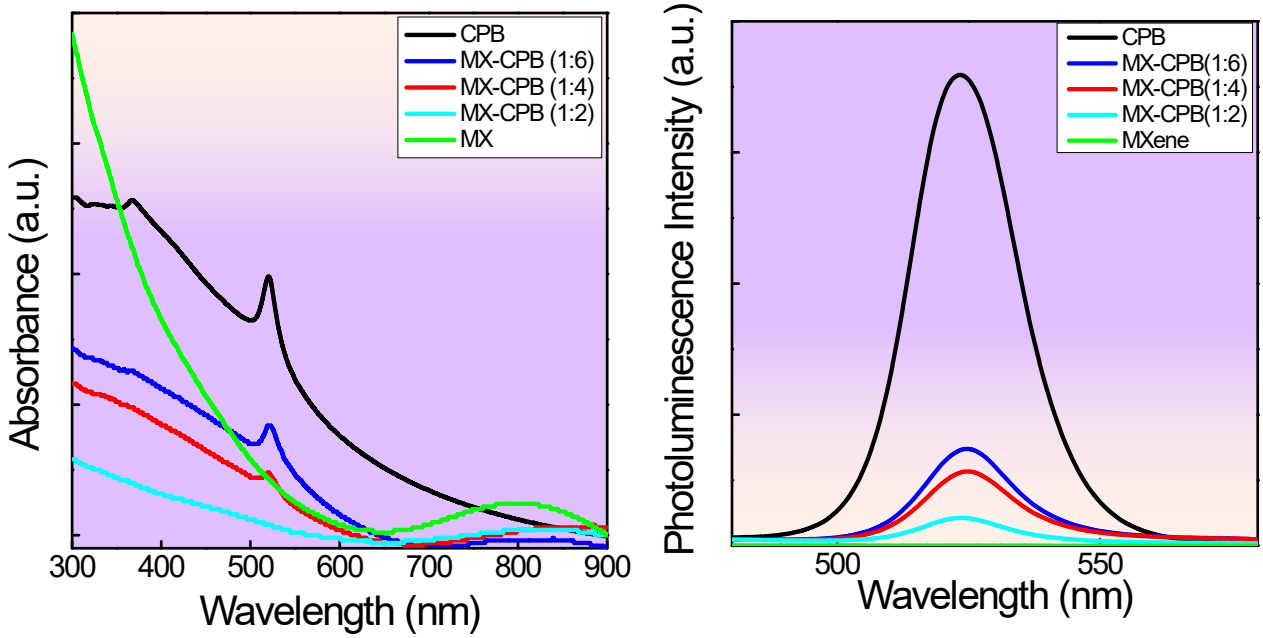

Figure S1: (a) Optical Absorbance, and (b) Steady state photoluminescence spectra of MXene-$CsPbBr_3$ nanocomposite with varying MX-CPB concentration.

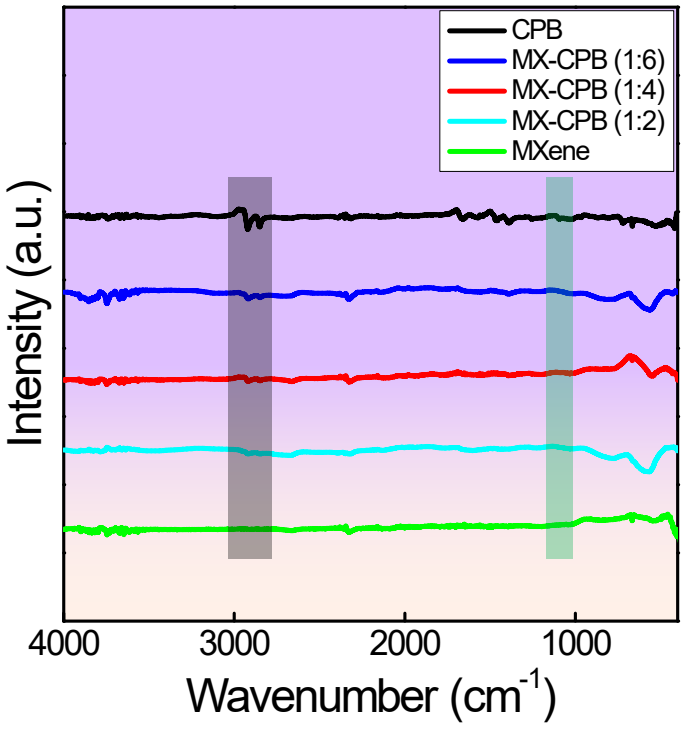

Figure S2: FTIR spectroscopy of MXene-$CsPbBr_3$ nanocomposite with varying MX-CPB concentration.

2. b) Structural analysis

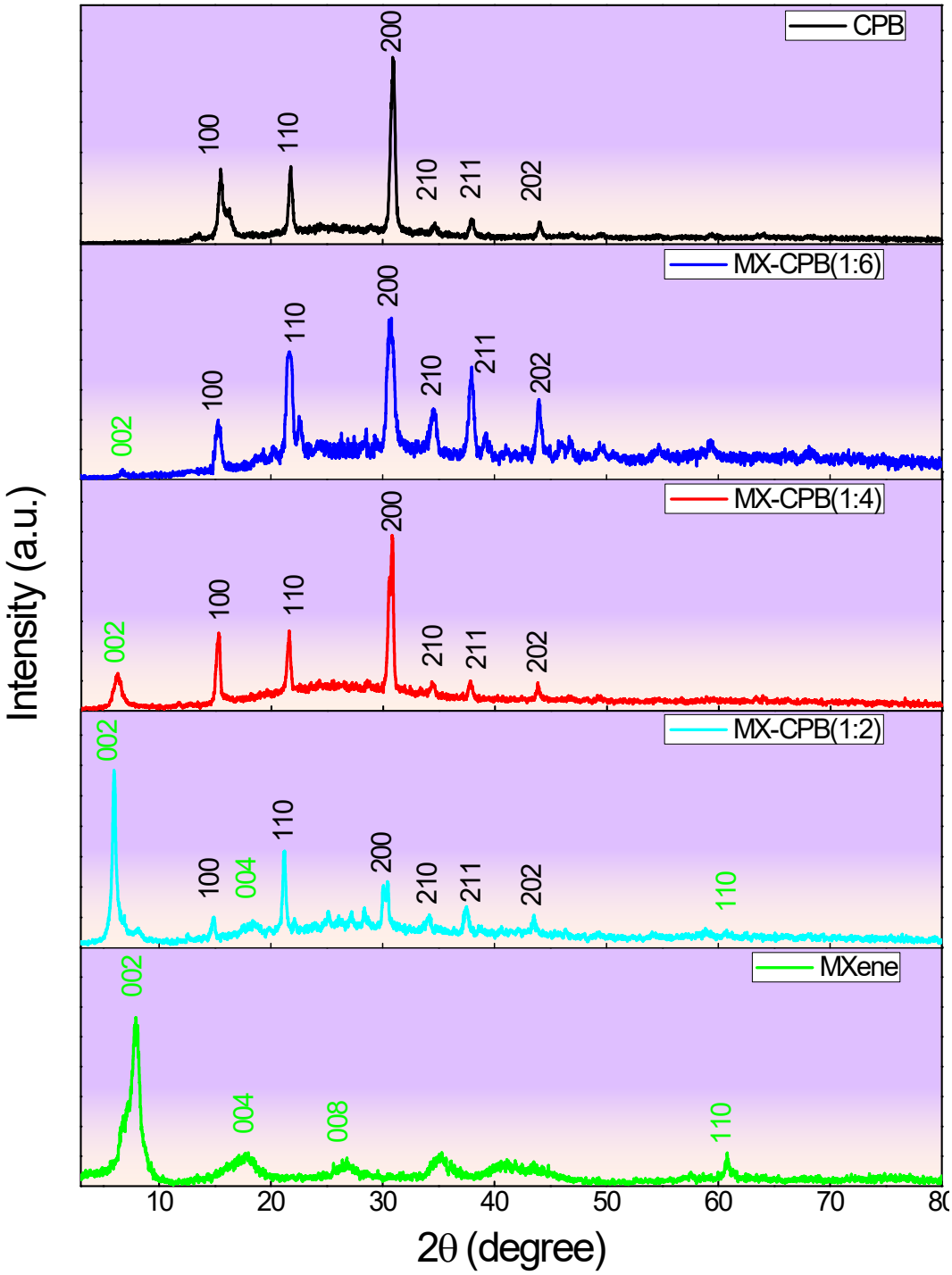

Figure S3: XRD spectra of MXene-$CsPbBr_3$ nanocomposite with varying MX-CPB concentration.

2.c) Morphological analysis

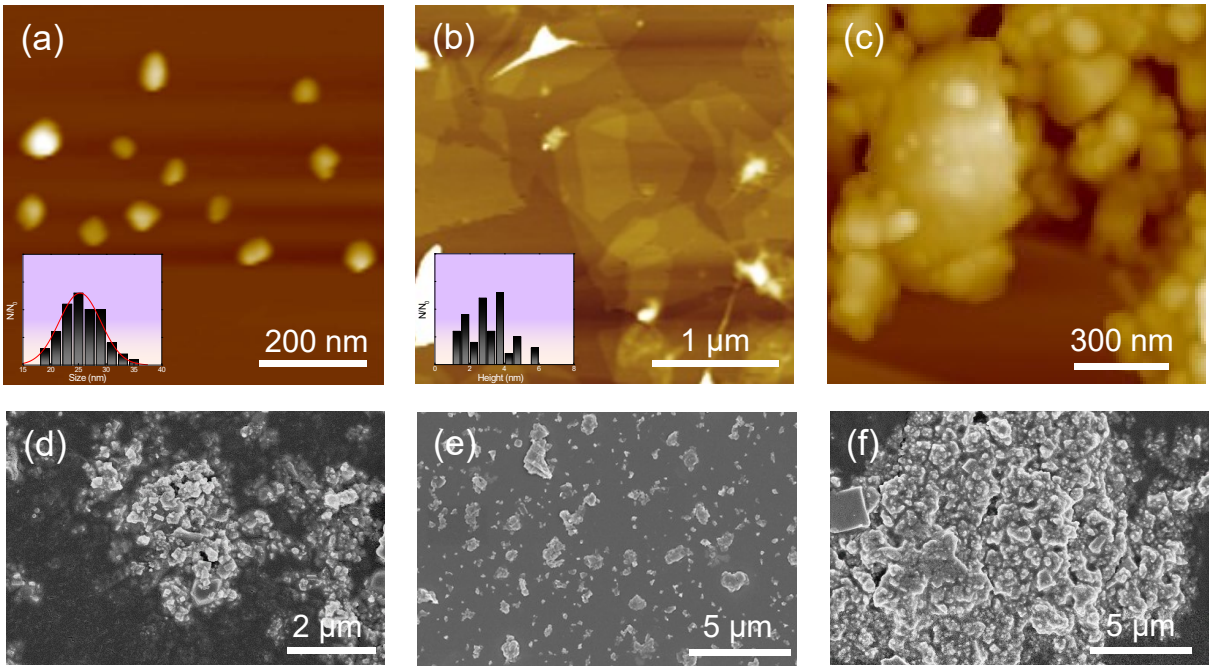

Figure S4: Morphological Properties of $CsPBBr_3$, pristine MXene, and MXene-CPB nanocomposites using AFM (a-c) and FESEM (d-f). Inset of (a): Size distribution of CsPbBr3 nanoparticle, and inset of (b): Size distribution of MXene.

2. d) XPS of Pristine CsPbBr3 and Ti3C2 MXene

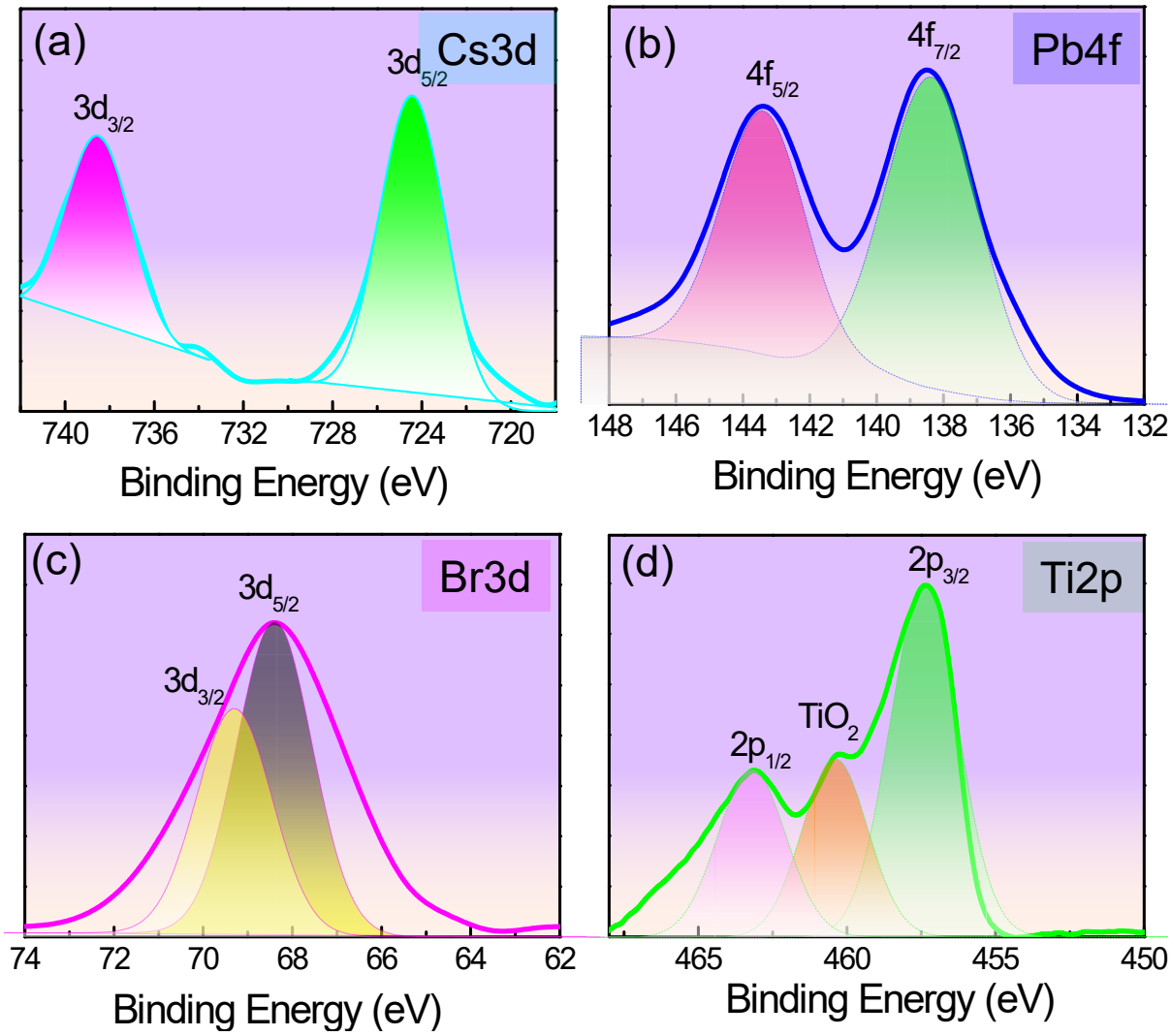

Figure S5: Core level XPS spectra of pristine $CsPbBr_3$ (a-c), and pristine Ti_3C_2 MXene (d).

3. Additional STS data

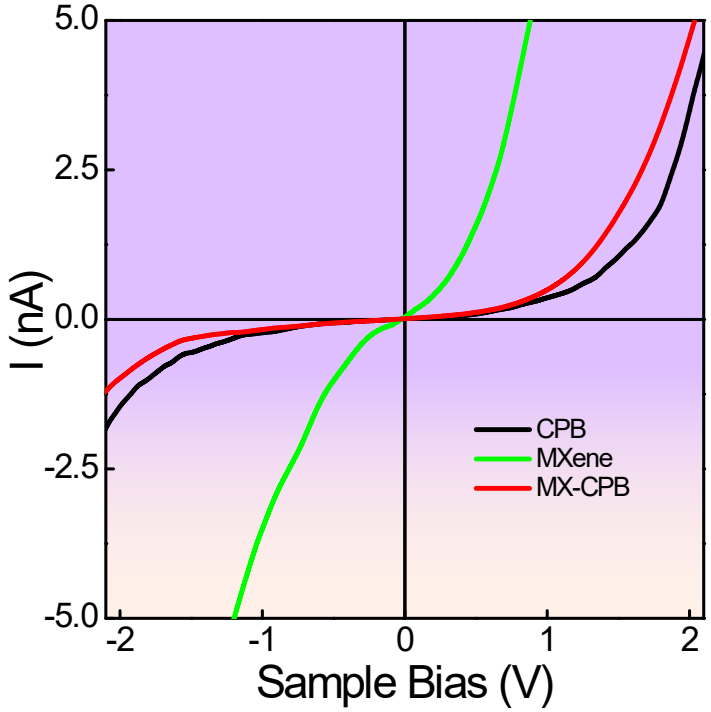

Figure S6: Tunneling current vs sample bias obtained from scanning tunneling spectroscopy data on pristine MXene, pristine CPB, and MX-CPB nanocomposite.

4. Additional EFM & KPFM data

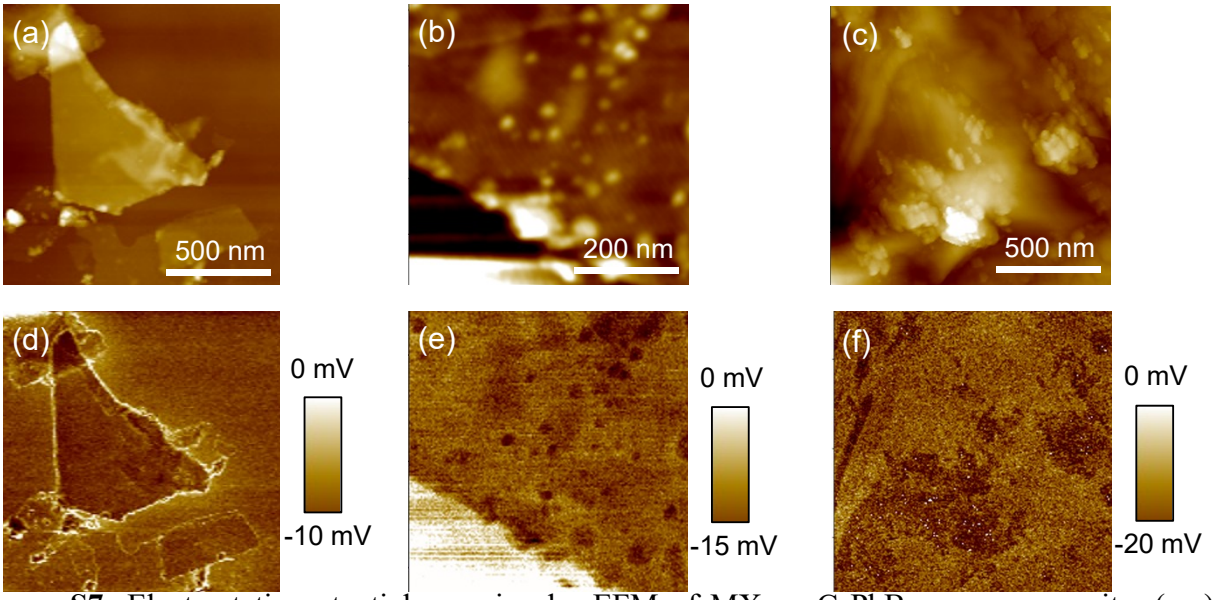

Figure S7: Electrostatic potential mapping by EFM of MXene-$CsPbBr_3$ nanocomposite: (a-c) EFM topographical image, and corresponding (d-f) amplitude image.

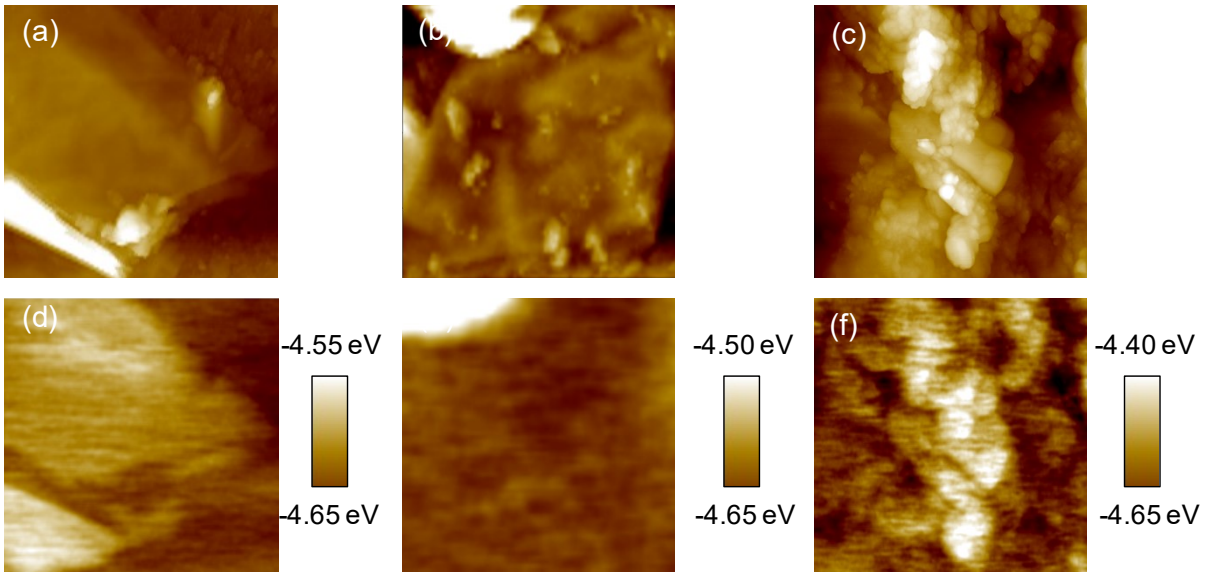

Figure S8: Surface potential mapping by KPFM of MXene-$CsPbBr_3$ nanocomposite: (a-c) KPFM topographical image, and corresponding (d-f) work-function signal.

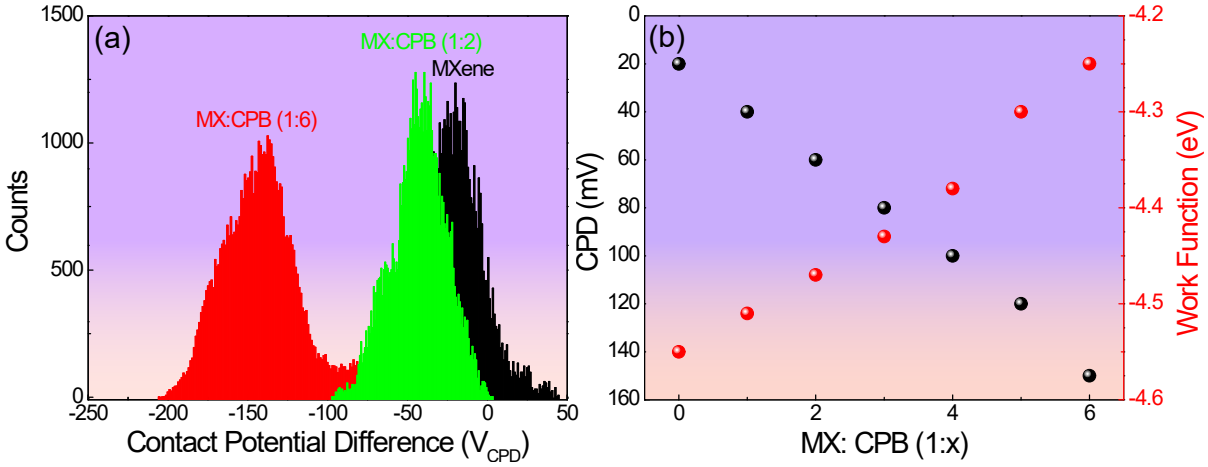

Figure S9: (a) Histogram profile and (b) surface potential and work-function modulation of MXene-$CsPbBr_3$ nanocomposite.

References

[1] X. Li, Y. Wu, S. Zhang, B. Cai, Y. Gu, J. Song, H. Zeng, Adv. Funct. Mater., 26 (2016) 2435-2445.

[2] W. Tian, A. VahidMohammadi, Z. Wang, L. Ouyang, M. Beidaghi, M.M. Hamedi, Nat. Commun., 10 (2019) 2558.